NANO LETTERS

2007
Vol. 7, No. 12
3716−3722

Modeling the Thermodynamics of the Interaction of Nanoparticles with Cell Membranes

Valeriy V. Ginzburg* and Sudhakar Balijepalli

Research and Development, The Dow Chemical Company, Building 1710, Midland, Michigan 48674

Received August 15, 2007; Revised Manuscript Received October 18, 2007

ABSTRACT

Interactions between nanoparticles and cell membranes may play a crucial role in determining the cytotoxicity of nanoparticles as well as their potential application as drug delivery vehicles or therapeutic agents. It has been shown that such interactions are often determined not by biochemical but by physicochemical factors (e.g., nanoparticle size, hydrophobicity, and surface charge density). Here, we propose a mesoscale thermodynamic model describing the transitions in membrane morphology observed after exposure to various types of nanoparticles. Our simulations demonstrate under which conditions (determined by particle size and hydrophilic/hydrophobic interactions) the particles can adsorb into the membrane or compromise the membrane integrity to result in the formation of nanosized holes. The model could be refined to include a more accurate description of various phospholipid membranes, and its results could be applied in the design of specific nanoparticles for various biomedical applications.

The use of nanoparticles in technology and medicine is rapidly increasing, and there have been a large number of studies aimed at examining and understanding the interactions between nanoparticles and human cells.[1−10] In some cases, nanoparticles can result in cytotoxicity, which can be beneficial (as in the cases when nanoparticles are used for cancer therapy[2−3]) or harmful.[4−6] Interestingly, several studies have shown that the effect of nanoparticles on cells often differs from that of microparticles even when chemical nature of the particulates is very similar.[5,6] It was further shown that nanoparticles can strongly interact with cell membranes, either adsorbing onto it[7−10] or compromising the membrane integrity to result in the formation of holes,[7−9] with the resulting morphology depending on the nanoparticle size and surface charge. In light of these observations, we propose that the mechanism of the changes in the membrane structure as a result of the interaction with nanoparticles can be ascribed to the lowering of the system free energy by making hybrid organic−inorganic micellar structures. To describe these new structures, we employ the Thompson−Ginzburg−Matsen−Balazs (TGMB) self-consistent field/density functional theory of block copolymer/nanoparticle mixtures,[11,12] adapting it to describe lipid bilayers (simplified representation of cell membranes) and nanoparticles in solution. We then map the new hybrid structures as a function of nanoparticle radius and surface treatment and qualitatively explain the observed trends.

* To whom the correspondence should be addressed. Email: vvginzburg@dow.com. Ph: (989) 636-9565.

We begin by writing down the free energy of a three-component mixture of water (W), diblock surfactant (D), and particle (P). Each diblock surfactant consists of a hydrophilic (H) block and lipophilic (L) block. Following the TGMB mean-field formalism, we write

$$\frac{FN_D}{k_BT\rho_0V} = f_1 + f_2 + f_3 + f_4 \quad (1)$$

$$f_1 = -\frac{\varphi_P}{\alpha}\ln\left(\frac{Q_P}{V}\right) - \varphi_D\ln\left(\frac{Q_D}{V}\right) - N_D\varphi_W\ln\left(\frac{Q_W}{V}\right)$$

$$f_2 = \frac{1}{V}\int \mathrm{dr}[\sum_{\alpha,\beta}(\chi_{\alpha\beta}N_D)\phi_\alpha(r)\phi_\beta(r) - \xi(r)(1 - \sum_\alpha \phi_\alpha(r))]$$

$$f_3 = \frac{1}{V}\int \mathrm{dr}[-\sum_{\alpha(\neq P)} w_\alpha(r)\phi_\alpha(r) - w_P(r)\rho_P(r)]$$

$$f_3 = \frac{1}{V}\int \mathrm{dr}[\rho_P(r)\Psi_{CS}(\bar{\phi}_P(r))] \quad (2)$$

Here, the first term, f_1, describes the "ideal mean-field" free energies of each component given external chemical potential fields w. The overall volume fractions of the components, φ_P, φ_D, and φ_W add up to 1. The partition functions of individual components, Q_P, Q_D, and Q_W, are defined in Appendix A. The second term, f_2, contains the (local) interactions among various species, described in a traditional Flory−Huggins[13,14] fashion, as well as the incompressibility constraint. The third term, f_3, contains the

10.1021/nl072053l CCC: $37.00
Published on Web 11/06/2007

terms with chemical potential fields w; note that, as in the original TGMB paper, the chemical potential fields are conjugate to the local volume fractions, $\phi_\alpha(\mathrm{r})$; the exception is the "particle" field, w_P, which is conjugate to the particle center density probability, $\rho_\mathrm{P}(\mathrm{r})$. Finally, the fourth term, f_4, contains the nonideal hard-sphere interactions, summed up via the "smoothed density approximation" of the hard sphere density functional theory (DFT) due to Tarazona.[15] In the Tarazona DFT, the nonideal free energy of the hard-sphere fluid is given by the Carnahan−Starling[16] equation of state

$$\Psi_{\mathrm{CS}}(x) = \frac{4x - 3x^2}{(1-x)^2} \tag{3}$$

In a sense, the particles are described by three interrelated "densities": center probability function, $\rho_\mathrm{P}(\mathrm{r})$; local volume fraction, $\phi_\mathrm{P}(\mathrm{r})$; and the "smoothed density" function, $\bar{\phi}_\mathrm{P}(\mathrm{r})$. The relationship between these three functions is as follows:

$$\phi_\mathrm{P}(\mathrm{r}) = \frac{1}{N_\mathrm{D}} \int \mathrm{d}\mathrm{r}'\rho_\mathrm{P}(\mathrm{r}')\Theta\left(1 - \frac{|\mathrm{r}-\mathrm{r}'|}{(R_\mathrm{P}/R_{\mathrm{gD}})}\right) \tag{4a}$$

$$\bar{\phi}_\mathrm{P}(\mathrm{r}) = \frac{1}{2^d N_\mathrm{D}} \int \mathrm{d}\mathrm{r}'\rho_\mathrm{P}(\mathrm{r}')\Theta\left(1 - \frac{|\mathrm{r}-\mathrm{r}'|}{(2R_\mathrm{P}/R_{\mathrm{gD}})}\right) \tag{4b}$$

Note that the spatial integration is in dimensionless coordinates scaled by the diblock radius of gyration, $R_{\mathrm{gD}} = a(N_\mathrm{D}/6)^{1/2}$. In introducing this scaling, we follow the formalism of Drolet and Fredrickson[17] whose real-space method of free energy minimization is adopted both in the TGMB paper and in this study. The power exponent d in eq 4b is space dimensionality, and Θ is the Heaviside step function ($\Theta(x) = 1$ if $x > 0$ and 0 otherwise).

Equation 1 determines the overall free energy of the system as a function of the local densities ($\phi_\alpha(\mathrm{r})$ for nonparticle species and $\rho_\mathrm{P}(\mathrm{r})$ for the particles), local chemical potentials $w_\alpha(\mathrm{r})$, and the incompressibility constraint field $\xi(\mathrm{r})$. Minimization of eq 1 with respect to all of these functions results in a set of self-consistency equations; these equations are then solved on a lattice using an iterative procedure until the specified convergence is achieved. In the original TGMB papers as well as in a recent study of hybrid nanoparticle/block copolymer micelles by Zhang et al.,[18] simulations began with random initial conditions. Here, we start from the field configuration representing a bilayer and a nanoparticle touching it on one side. Also, in our study we consider the case of a single "stationary" nanoparticle, while the other papers dealt with ensemble of nanoparticles. The particle is "created" by setting $w_\mathrm{P}(\mathrm{r})$ as a sharp Gaussian (almost a delta-function) with maximum at the particle center; then, because of eq 4a and the incompressibility constraint, $\phi_\mathrm{P}(\mathrm{r}) \approx 1$ within the d-dimensional sphere of radius R_P ($d = 2$ or 3 is the space dimensionality of the simulation box; in our system, $d = 2$). Over the course of the simulation, $w_\mathrm{P}(\mathrm{r})$ is kept constant, while all other variables are driven toward the state corresponding to the local free energy minimum. Thus, unlike earlier studies of thermodynamics of "hard" stationary particles in multicomponent polymer blends or solutions (see, e.g., Reister and Fredrickson[19]), there is no need to explicitly enforce boundary conditions on the particle surface. For more details on the algorithm, see Appendix A.

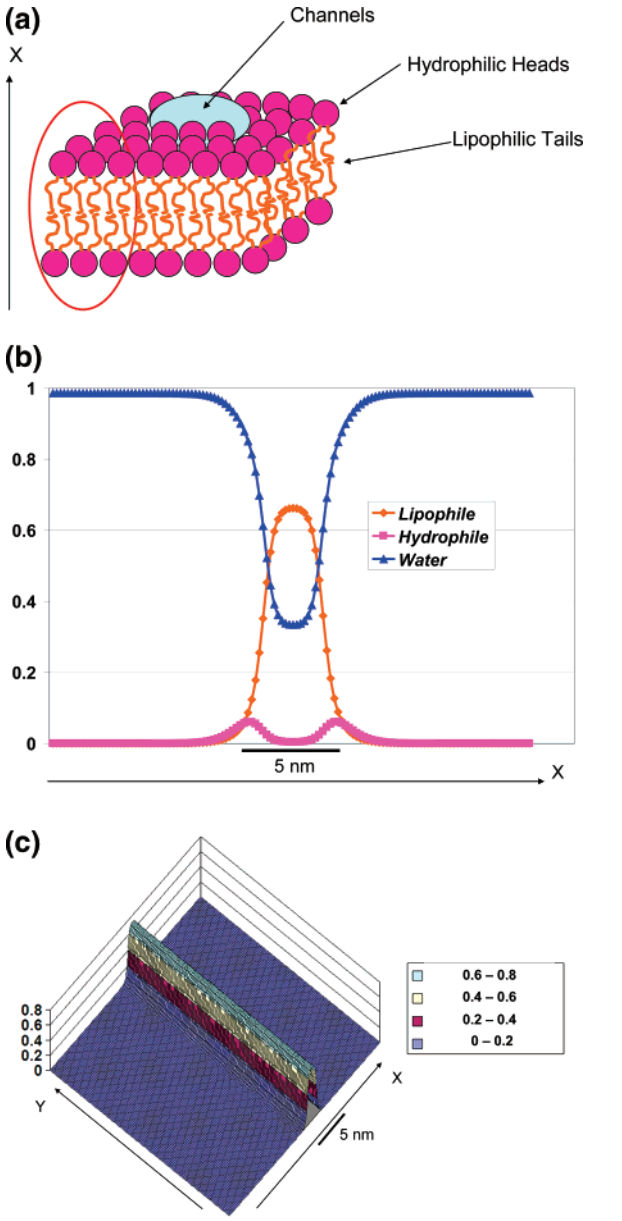

Figure 1. Simplified representation of a cell membrane: (a) sketch of the membrane structure; (b) simulated density profiles of various species as function of the distance from the center of the bilayer; (c) simulated density map of the lipophilic part of the bilayer. X-axis represents the normal to the membrane plane.

We begin by simulating a particle-free solution of phospholipids in water, starting from the uniform initial condition. Our goal is to obtain a phospholipid bilayer that would give reasonable representation of a cell membrane (see Figure 1a). A typical phospholipid surfactant has a hydrophilic headgroup and one or two lipophilic tails. We model it as a simple diblock with hydrophilic (H) and lipophilic (L) blocks. The total degree of polymerization is denoted N_D, and the fraction of lipophilic block is denoted f. We assume that each segment has Kuhn length $a = 0.4$ nm, and volume $(\rho_0)^{-1} = 0.064$ nm^3. The volume fraction of the diblock is denoted

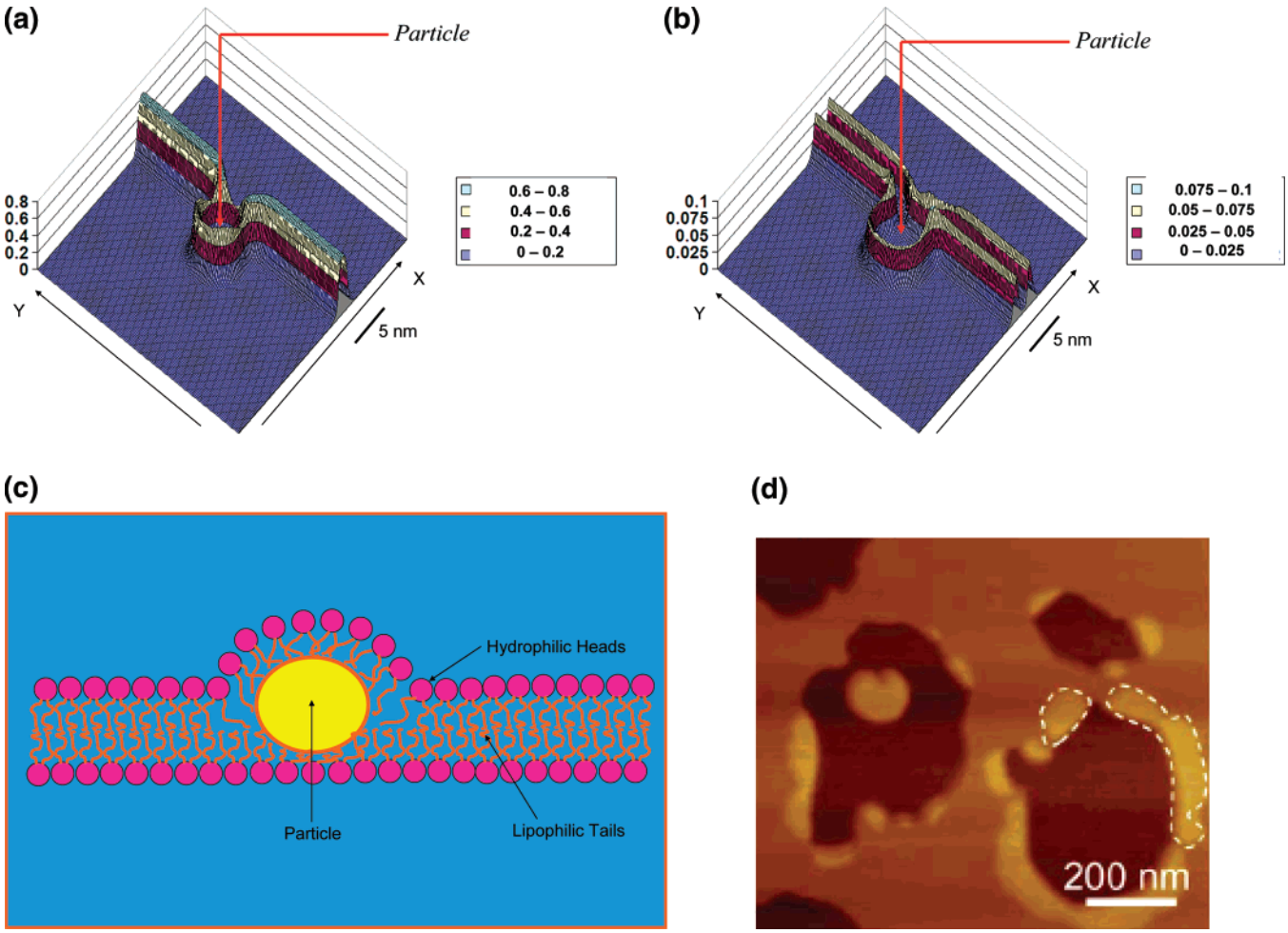

Figure 2. Nanoparticles adsorbed into the cell membrane. (a) Simulated density map of the lipophilic part of the bilayer. (b) Simulated density map of the hydrophilic (headgroup) part of the bilayer. *X*-axis is normal to the bilayer plane. (c) Sketch demonstrating the molecular arrangements in the nanoparticle-bilayer complex. (d) Atomic force microscope (AFM) pictures of lipid bilayers with adsorbed charge-neutralized PAMAM dendrimers (reprinted with permission from ref 8, copyright American Chemical Society, 2004). Particle radius R_p = 2.4 nm.

φ_D, while the rest of the system is water (W). The morphology of the membrane is determined by N_D and φ_D, as well as by the pairwise Flory−Huggins interaction parameters, χ_{HL}, χ_{WL}, and χ_{HL}. Here, we take $\chi_{HL} = \chi_{WL} = 1.0$, $\chi_{HL} = 0.0$, $N_D = 50$, $f = 0.88$, and $\varphi_D = 0.05$. Simulated density profiles (local volume fractions) of hydrophilic (H) and lipophilic (L) blocks, as well as water (W) are shown in Figure 1b. It can be seen that our model successfully captures many features of a typical cell membrane; a slight drawback is that it somewhat overestimates the fraction of water inside the bilayer. The thickness of the membrane that "self-assembles" in our simulation is approximately 16 lattice cells $= 14.4a \sim 5.6$ nm, which is consistent with the thickness of, for example, dimyristoylphosphatidylcholine (DMPC) membrane.[9] In Figure 1c, we plot the density map of the lipophilic block; because the volume fraction of lipophiles in the membrane is almost 90%, it is a good indication of the morphology of the whole membrane, and will be the basis of comparison as we evaluate the changes brought by the particle.

We can now model the thermodynamics of the nanoparticle/membrane interaction. To do that, we save all the fields from the final configuration representing the bilayer and then add the new field describing the particle. The particle field is set up as a sharp Gaussian with maximum being exactly one particle radius away from the outer edge of the bilayer. We then use the new fields as the starting point for the simulations. To facilitate comparison with experimental studies (for example, recent studies by Banaszak Holl, refs 7−9), we fix the Flory−Huggins interaction parameters between the particle and water, $\chi_{PW} = 1.0$, and particle and lipid, $\chi_{PL} = 0.0$, while varying the interaction parameter between the particle and the headgroup, χ_{PH}, from +1.0 (repulsive) to −3.0 (strongly attractive). This variation is expected to mimic the role of the nanoparticle surface charges. The uncharged particles ($\chi_{PH} = +1.0$) should show hydrophobic tendencies, while strongly charged particles ($\chi_{PH} = -3.0$) should have attractive interactions with the zwitterionic (dipolar) headgroups.[20] The simulation results (final morphologies after 10 000 iterations) are depicted in Figure 2a,b (for uncharged particles of radius $R = 2.4$ nm) and Figure 3a,b (for strongly charged particles of the same radius).

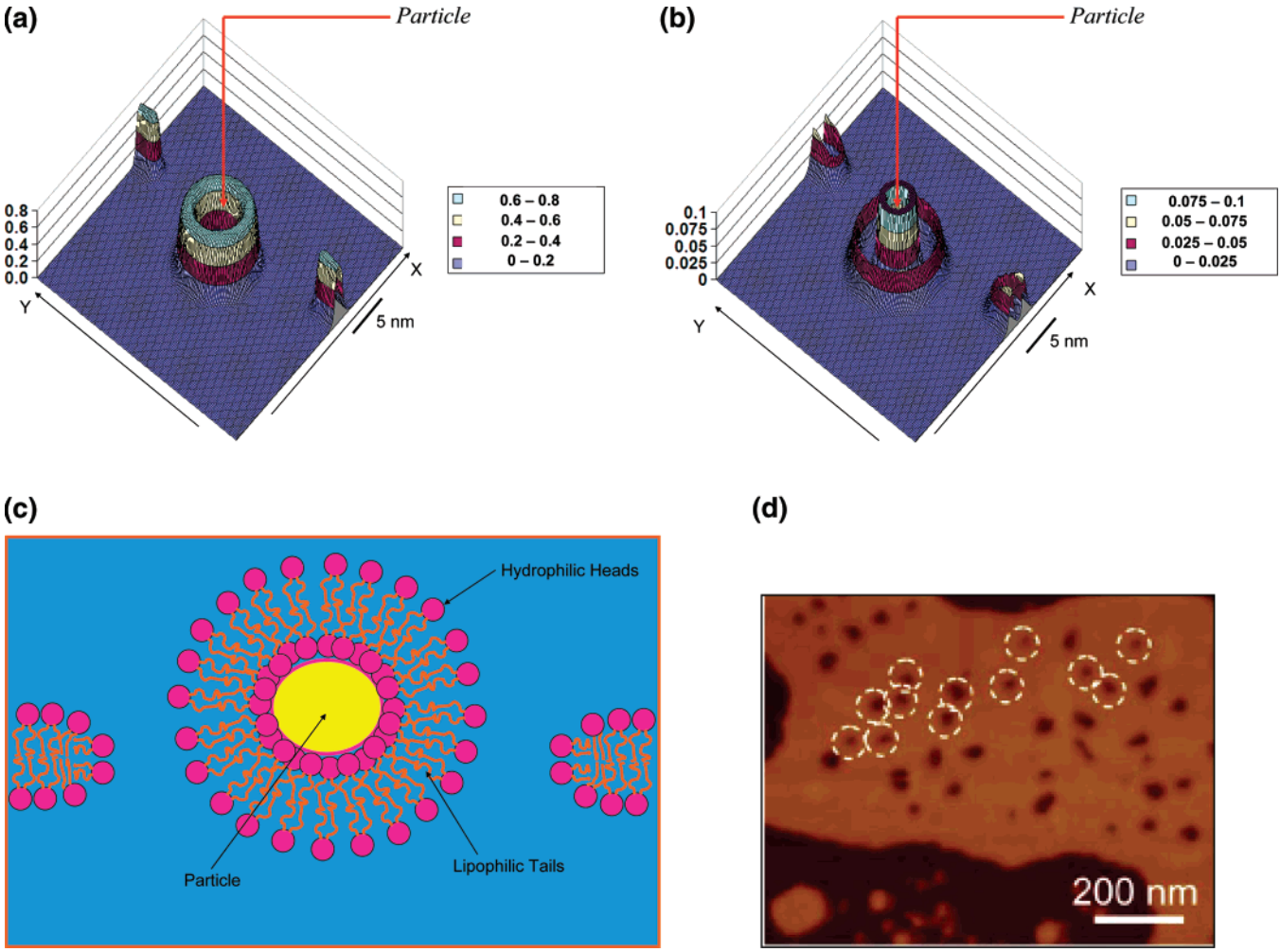

Figure 3. Nanoparticles causing hole formation in the cell membrane. (a) Simulated density map of the lipophilic part of the bilayer. (b) Simulated density map of the hydrophilic (headgroup) part of the bilayer. *X*-axis is normal to the bilayer plane. (c) Sketch demonstrating the formation of a nanoparticle-bilayer complex and corresponding breakage of the original membrane. (d) AFM pictures of lipid bilayers with holes made by charged PAMAM dendrimers (reprinted with permission from ref 8, copyright American Chemical Society, 2004). Particle radius $R_p = 2.4$ nm.

We first consider uncharged ("hydrophobic") nanoparticles. In this case, the particle is likely to be absorbed into the membrane, swelling it and effectively "cleaving" its internal hydrophobic bilayer into two. This mechanism is somewhat similar to the selective swelling of block copolymer lamellar domains by nanoparticles.[11,12] By inspecting the density maps for lipids (Figure 2a) and headgroups (Figure 2b), we can see that the particle is indeed lodged in the middle of the lipid bilayer. The proposed mechanism of the particle incorporation into the membrane is sketched in Figure 2c. Because of the hydrophobic nature of the particle surface, the particle breaks up the bilayer to increase its contacts with the lipophilic surfactant tails and thereby minimize its surface tension. Such behavior is consistent with recent experiments by Banaszak Holl[7−9] showing that charge-neutral PAMAM dendrimers G5-Ac absorb to the existing supported lipid bilayers (Figure 2d); the layers thicken, but no new holes are formed.

The behavior of the membrane changes completely in the presence of strongly charged nanoparticles. Because of the strong attraction of the headgroups to the particle surface, the preferential phospholipid arrangement now would be to form a bilayer around the particle. The density maps for lipids (Figure 3a) and headgroups (Figure 3b) both support this hypothesis. As a result of this, large numbers of phospholipid molecules are pulled away from the original membrane. The membrane then can thin or even rupture. In the particular simulation represented in Figure 3, we observe the rupture of the membrane and the formation of a hole. The mechanism of the corresponding structural change is illustrated in Figure 3c. This model is consistent with the hole formation observed by Banaszak Holl[7−9] in the systems where supported lipid bilayers were exposed to charged PAMAM dendrimers G7-NH_2 (Figure 3d). Indeed, Banaszak Holl and co-workers speculated that the hole formation in the bilayers was caused by a migration of phospholipids onto the dendrimer (or other charged nanoparticle) surface and the formation of "dendrimer-filled vesicles".[7]

From the above analysis, it follows that uncharged or hydrophobically modified nanoparticles can incorporate into cell membranes resulting in membrane swelling. On the other hand, strongly charged or more hydrophilic nanoparticles can pull the phospholipids away from the membrane, forming a hybrid micelle (particle as the core, phospholipid bilayer as the shell). This process can lead to the rupture of the original membrane and the formation of nanosized holes.

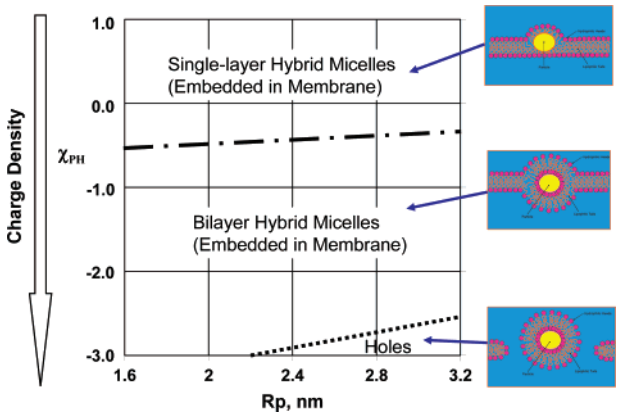

Figure 4. Phase diagram illustrating the nature of membrane/nanoparticle interaction as a function of particle surface treatment and particle size.

To qualitatively understand the dependence of the particle/membrane interaction on particle size and surface treatment type, we carried several simulations with various particle radii (R_p = 1.6, 2.0, 2.4, 2.8, and 3.2 nm) and particle-hydrophile interaction parameters (χ_{PH} = 1.0, 0.0, −1.0, −2.0, −3.0). The results of these simulations are summarized in the phase diagram shown in Figure 4. It can be seen that as the charge density of the particle surface is increased, the particle is attracting more and more phospholipid molecules away from the membrane so that they could adsorb on the particle surface. In particular, while the neutral particles surround themselves with a monolayer of phospholipids, the strongly charged particles have to surround themselves with a bilayer, thus taking away twice as much phospholipids as the neutral ones. This qualitative picture is also supported by the analysis of density profiles across the particle and the membrane in the *X*-direction (perpendicular to the membrane surface), plotted in Figure 5. It can be seen that while for the "neutral" (χ_{PH} = 1.0) nanoparticles (Figure 5a,c,e), there are only two maxima in the headgroup (H) density profile (pink curves), indicating that the particle goes inside the bilayer and swells it. On the other hand, for the "charged" (χ_{PH} = −3.0) particles (Figure 5b,d,f), there are four maxima for the headgroup density profile. This indicates that the particles attract the headgroups and cause the phospholipids to attempt to create a curved bilayer around the particle. Ultimately, if the particles are sufficiently large, they attract so much phospholipid that the membrane can no longer sustain its flat morphology and reduces its free energy by making a hole. Thus, one can observe the creation of holes in the case of strongly charged particles whose diameter is comparable or larger than the membrane thickness, as demonstrated by Banaszak Holl[7−9]

So far, our analysis concentrated on nanoparticles with $R_p \sim 1-4$ nm. What could be expected if the nanoparticle size is increased? We believe that the same trends would be observed for slightly larger sizes ($R_p \sim 5-10$ nm) where particle size is still comparable to the membrane thickness. One could imagine that within this range, neutral nanoparticles would still be able to incorporate into the membrane, while charged ones would be forcing hole formation. As particle size becomes larger, the activation barriers for these processes (due to the disruption of the bilayer) are likely to increase substantially (proportionally to the particle surface area). It is still possible that strongly charged particles could overcome those barriers and pull the phospholipids away from the membrane as discussed above. This could be done, for example, through the mechanism discussed by Deserno and Gelbart[21] and Smith et al.[22] where the membrane first wraps around the particle and then the coated particle can detach from the original membrane. For large neutral particles, the activation barrier might be too difficult to overcome, and the membrane conformation might remain intact.

It is important to point out that our model addresses only thermodynamic aspects of the particle/membrane interactions. To better understand this interaction, dynamical models such as Dissipative Particle Dynamics[22,23] could be used. Those models could help shed light on the activation barriers and characteristic times for the particle absorption into the membranes (for neutral, hydrophobic particles) or for the particle movement through the membranes (for charged particles).

Further extensions and generalizations of the method described here could be developed to account for various (more or less hydrophobic) types of particle surface treatments, particle surface charges, and particle shape anisotropy. Using this or similar mesoscale approach, it should become possible to map out the "equilibrium" outcomes of nanoparticle/cell membrane interactions as function of particle characteristics. Those maps in turn could be helpful in a variety of areas from predicting nanoparticle cytotoxicity to improving design of drug and gene delivery vehicles in a rapid, high-throughput fashion.

Acknowledgment. This work was supported by The Dow Chemical Company. We thank Drs. D. Boverhof, B. Gollapudi, L. Hong, C. Christenson, T. Thompson, M. Debney (Dow), M. Banaszak Holl, B. Orr, P. Leroueil, and Mr. C. Kelly (University of Michigan) for helpful discussions. We are indebted to Dr. K. Smith and Professor A. C. Balazs for sharing with us ref 22 prior to publication.

Appendix A. Self-Consistency Equations and Simulation Details

Partition functions of individual components are given by

$$Q_W = \int \exp\{-w_W(r)\}\, dr \quad \text{(A1)}$$

$$Q_P = \int \exp\{-w_P(r)\}\, dr \quad \text{(A2)}$$

$$Q_D = \int q(r,1)\, dr \quad \text{(A3)}$$

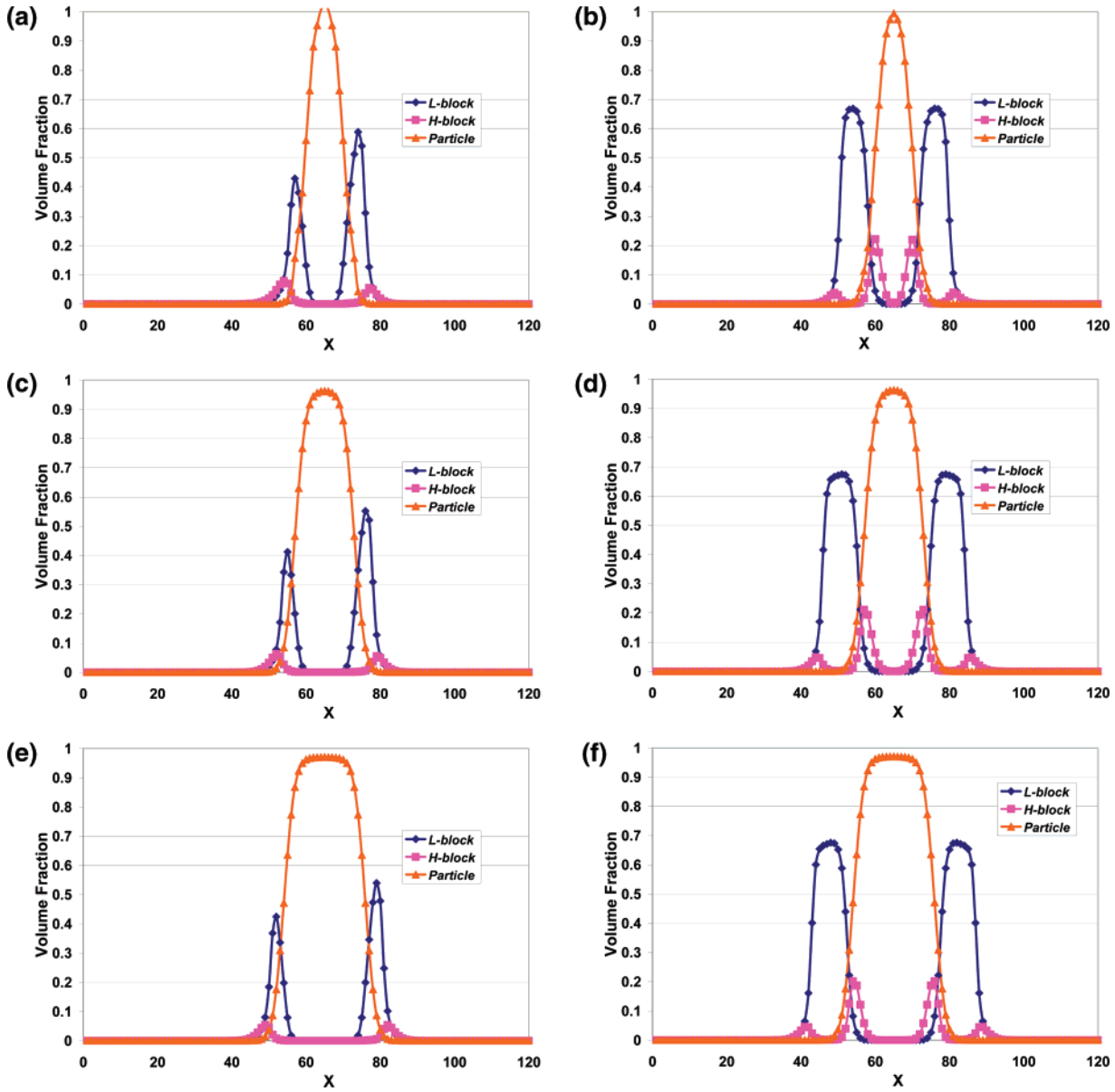

Figure 5. Density profiles for hydrophilic (H) and lipophilic (L) blocks of the membrane surfactant, as well as particles, along the line normal to the original membrane surface and passing through the nanoparticle center. Cases considered: (a) $R_P = 1.6$ nm, $\chi_{PH} = 1.0$; (b) $R_P = 1.6$ nm, $\chi_{PH} = -3.0$; (c) $R_P = 2.4$ nm, $\chi_{PH} = 1.0$; (d) $R_P = 2.4$ nm, $\chi_{PH} = -3.0$; (e) $R_P = 3.2$ nm, $\chi_{PH} = 1.0$; (f) $R_P = 3.2$ nm, $\chi_{PH} = -3.0$. X-scale: 1 lattice unit = 0.36 nm.

Here, the propagator $q(r, s)$ (where $0 < s < 1$ is the index denoting the position along the diblock chain) and its counterpart $q\dagger(r, s)$ are given by the modified diffusion equations

$$\frac{\partial q(r,s)}{\partial s} = [\nabla^2 - w_{t(s)}]q(r,s) \qquad \text{(A4a)}$$

$$\frac{\partial q\dagger(r,s)}{\partial s} = -[\nabla^2 - w_{t(s)}]q\dagger(r,s) \qquad \text{(A4b)}$$

Here, $t(s) = L$ if $s < f$, and H otherwise. Equations A4a and A4b have to be solved subject to boundary conditions $q(r, 0) = q\dagger(r, 1) = 1$.

The self-consistency equations are obtained by differentiating eq 1 with respect to $\phi_H(r)$, $\phi_L(r)$, $\phi_W(r)$, $\rho_P(\boldsymbol{r})$, $w_H(r)$, $w_L(r)$, $w_W(r)$, $w_P(r)$, and $\xi(r)$.

$$w_H(r) = \chi_{HL}N_D\phi_L(r) + \chi_{HP}N_D\phi_P(r) + \xi(r) \qquad \text{(A5a)}$$

$$w_L(r) = \chi_{HL}N_D\phi_H(r) + \chi_{WL}N_D\phi_W(r) + \xi(r) \qquad \text{(A5b)}$$

$$w_W(r) = \chi_{WL}N_D\phi_L(r) + \chi_{WP}N_D\phi_P(r) + \xi(r) \qquad \text{(A5c)}$$

$$w_P(r) = \Psi_{CS}(\bar{\phi}_P(r)) + \frac{1}{N_D}\int dr'\, \Theta\left(1 - \frac{|r - r'|}{(R_P/R_{gD})}\right) \times [\chi_{HP}N_D\phi_H(r') + \chi_{WP}N_D\phi_W(r') + \xi(r')] + \frac{1}{2^d N_D}\int dr'\, \Theta\left(1 - \frac{|r - r'|}{(2R_P/R_{gD})}\right) \times [\rho_P(r')\Psi'_{CS}(\bar{\phi}_P(r'))] \qquad \text{(A5d)}$$

$$\rho_P(r) = \frac{\varphi_P}{\alpha}\frac{V}{Q_P}\exp[-w_P(r)] \quad \text{(A5e)}$$

$$\phi_W(r) = \varphi_W\frac{V}{Q_P}\exp[-w_W(r)] \quad \text{(A5f)}$$

$$\phi_L(r) = \varphi_D\frac{V}{Q_D}\int_0^f q(r,s)q\dagger(r,s)\,ds \quad \text{(A5g)}$$

$$\phi_H(r) = \varphi_D\frac{V}{Q_D} > \int_f^1 q(r,s)q\dagger(r,s)\,ds \quad \text{(A5h)}$$

$$\phi_H(r) + \phi_L(r) + \phi_P(r) + \phi_W(r) = 1 \quad \text{(A5i)}$$

Equations A5a−i, together with definitions of functions $\phi_P(r)$ and $\bar{\phi}_P(r)$ (eqs 4a and 4b), constitute a full set of self-consistency equations that need to be solved iteratively. The solution algorithm, adapted from the approach of Drolet and Fredrickson[17] and the original TGMB paper[11], is as follows. First, the chemical potential and pressure fields are initialized. Next, using eqs A5e−i together with eqs 4a and 4b, density fields for all species are calculated. Then, new chemical potential fields are generated using the Drolet−Fredrickson prescription

$$w_i^{t+1}(r) = (1 - \lambda_i)w_i^t(r) + \lambda_i\mu_i(r) \quad \text{(A6)}$$

where t is the iteration number ("effective time"), i = H, L, W, or P, λ_i is the "time step", and μ_i are the "new chemical potentials" calculated using eqs A5a−d. Finally, we update the pressure field, ξ, using the following formula

$$\xi(r) = \hat{F}^{-1}(P(q)) + \epsilon(\phi_P(r) + \phi_W(r) + \phi_H(r) + \phi_L(r) - 1) \quad \text{(A7a)}$$

$$P(q) = \frac{H_W(q) + H_P(q) + H_H(q) + H_L(q)}{3 + N_D^{-1}\hat{F}\left(\Theta\left(1 - \frac{r}{[R_P/R_{gD}]}\right)\right)} \quad \text{(A7b)}$$

Functions $H_H(q)$, $H_L(q)$, $H_W(q)$, and $H_P(q)$ are Fourier transforms of the right-hand sides of eqs A5a−d, respectively, except for the terms containing ξ. Operators $\hat{F}$ and $\hat{F}^{-1}$ denote the standard (either two- or three-dimensional) Fourier transforms. (Note that eqs A7a and A7b can be used only in conjunction with periodic boundary conditions).

Equations A7a and A7b conclude the description of the (slightly modified) TGMB model. In our study, we fix the particle field by setting the initial condition

$$w_P(i,j) = -A\exp[-B\{(i - I)^2 + (j - J)^2\}] \quad \text{(A8)}$$

where (i,j) are local coordinates of a given point r, (I, J) are coordinates of the particle center, and A and B are large numbers so that eq A8 effectively represents a delta-function (we used $A = 10.0$, $B = 10.0$). We then keep the initial particle field constant throughout the simulation by setting $\lambda_P = 0$, while all the other fields are minimized with the same "time step" λ. In addition, the equation for the pressure field, A7, is modified as follows

$$\xi(r) = P(r) + \epsilon(\phi_P(r) + \phi_W(r) + \phi_H(r) + \phi_L(r) - 1) \quad \text{(A9a)}$$

$$P(r) = \frac{H_W(r) + H_H(r) + H_L(r)}{3} \quad \text{(A9b)}$$

where $H_H(r)$, $H_L(r)$, and $H_W(r)$ are the right-hand sides of eqs A5a−c, respectively, except for the terms containing ξ.

We set $\lambda = 0.025$, and $\epsilon = 60$. With these parameters, we obtained reliable convergence for all particle radii in the range $4a < R_p < 8a$; the average deviation from the incompressibility, $|\sum\phi - 1|$, was less than 10^{-3} in all cases.

References

(1) Salata, O. J. *Nanobiology* **2004**, *2*, 3 and references therein.
(2) El-Sayed, I. H.; Huang, X.; El-Sayed, M. A. *Nano Lett.* **2005**, *5*, 829.
(3) Ferrari, M. *Nat. Rev. Cancer* **2005**, *5*, 161 and references therein.
(4) Nel, A.; Xia, T.; Mädler, L.; Li, N. *Science* **2006**, *311*, 622 and references therein.
(5) Rothen-Rutishauser, B. M.; Schürch, S.; Haenni, B.; Kapp, N.; Gehr, P. *Environ. Sci. Technol.* **2006**, *40*, 4353.
(6) Brunner, T. J.; Wick, P.; Manser, P.; Spohn, P.; Grass, R. N.; Limbach, L. K.; Bruinink, A.; Stark, W. J. *Environ. Sci. Technol.* **2006**, *40*, 4374.
(7) Mecke, A.; Majoros, I. J.; Patri, A. K.; Baker, J. R., Jr.; Banaszak Holl, M. M; Orr, B. G. *Langmuir* **2005**, *21*, 10348.
(8) Hong, S.; Bielinska, A. U.; Mecke, A.; Kezsler, B.; Beals, J. L.; Shi, X.; Balogh, L.; Orr, B. G.; Baker, J. R., Jr.; Banaszak Holl, M. M. *Bioconjugate Chem.* **2004**, *15*, 774.
(9) Leroueil, P. R.; Hong, S.; Mecke, A.; Baker, J. R., Jr.; Banaszak Holl, M. M; Orr, B. G. *Acc. Chem. Res.* **2007**, *40*, 335 and references therein.
(10) Zhang, L.; Granick, S. *Nano Lett.* **2006**, *6*, 694.
(11) Thompson, R. B.; Ginzburg, V. V.; Matsen, M. W.; Balazs, A. C. *Science* **2001**, *292*, 2469.
(12) Thompson, R. B.; Ginzburg, V. V.; Matsen, M. W.; Balazs, A. C. *Macromolecules* **2002**, *35*, 1060.
(13) Huggins, M. L. *J. Chem. Phys.* **1941**, *9*, 440.
(14) Flory, P. J. *J. Chem. Phys.* **1941**, *9*, 660.
(15) Tarazona, P. *Mol. Phys.* **1984**, *52*, 81.
(16) Carnahan, N. F.; Starling, K. E. *J. Chem. Phys.* **1969**, *51*, 635.
(17) Drolet, F.; Fredrickson, G. H. *Phys. Rev. Lett.* **1999**, *83*, 4317.
(18) Zhang, L.; Lin, J.; Lin, S. *Macromolecules* **2007**, *40*, 5582.
(19) Reister, E.; Fredrickson, G. H. *Macromolecules* **2004**, *37*, 4718.
(20) Strictly speaking, introduction of charged groups onto the particle surfaces should change all three Flory−Huggins parameters, χ_{PH}, χ_{PL}, and χ_{PW}. To accurately calculate Flory−Huggins parameters, especially for charged systems, remains a daunting task requiring extensive molecular simulations and is beyond the scope of this study. We assumed here that the introduction of charged groups to functionalize the surface of the otherwise hydrophobic particles would have the strongest impact on the particle interaction with the headgroups; hence, this study maps out the phase diagram as function of χ_{PH} while leaving the other two parameters constant. More detailed analysis would be required to map out the phase diagram as function of all three parameters, χ_{PH}, χ_{PL}, and χ_{PW}.
(21) Deserno, M.; Gelbart, W. M. *J. Phys. Chem. B* **2002**, *106*, 5543.
(22) Smith, K. A.; Jasnow, D.; Balazs, A. C. *J. Chem. Phys.* **2007**, *127*, 084703.
(23) Yamamoto, S.; Maruyama, Y.; Hyodo, S. *J. Chem. Phys.* **2002**, *116*, 5842.

NL072053L